Collisionless expansion of pulsed rf plasmas II: Parameter study

T Schröder,[1] O Grulke,[1] T Klinger,[1,2] R W Boswell,[3] and C Charles[3]
[1)] *Max-Planck-Institute for Plasma Physics, Greifswald, Germany*
[2)] *Ernst-Moritz-Arndt-University, Greifswald, Germany*
[3)] *Space Plasma, Power and Propulsion Group, Research School of Physical Sciences and Engineering, The Australian National University, Australian Capital Territory 0200, Australia*

The plasma parameter dependencies of the dynamics during the expansion of plasma are studied with the use of a versatile particle-in-cell simulation tailored to a plasma expansion experiment[1,2]. The plasma expansion into a low-density ambient plasma features a propagating ion front that is preceding a density plateau. It has been shown that the front formation is entangled with a wave-breaking mechanism, i.e. an ion collapse[3,4], and the launch of an ion burst[2]. The systematic parameter study presented in this paper focuses on the influence on this mechanism its effect on the maximum velocity of the ion front and burst.

It is shown that, apart from the well known dependency of the front propagation on the ion sound velocity, it also depends sensitively on the density ratio between main and ambient plasma density. The maximum ion velocity depends further on the initial potential gradient, being mostly influenced by the plasma density ratio in the source and expansion region. The results of the study are compared to independent numerical studies.

PACS numbers: 5275Di, 5259Dk, 5259Fn
Keywords: plasma acceleration, plasma expansion, PIC simulation

I. INTRODUCTION

The investigation of plasmas expanding into vacuum is ongoing for decades. in order to describe the plasma behaviour around supersonic satellites, during coronal mass ejections or super novas. A number of the theoretical approaches have focussed their investigation on the temporal evolution of an initially step-like (semi-infinite) ion density profile in collisionless, hydrodynamic regimes. Such setups have been shown to evolve into self-similar density profiles[5–10]. These approaches, however, converge towards different physical limits. As such, the maximum expansion velocities vary on a scale from the ion sound velocity c_i[7–9] up to the electron thermal velocity v_e[5,6]. Various experiments have been carried out in thermionic discharges[11,12], fireballs[13], and laser produced plasmas[14–16]. They yield that the expansion velocities depend strongly on the electron energy distribution[16–20]. In particular, the ion acceleration is expected to be enhanced by non-thermal electrons[11,21].

In this work a particle-in-cell (PIC) simulation is used that has been tailored to a pulsed rf plasma expansion experiment[1]. The simulation can qualitatively reproduce the experimental results[2]. It allows for a systematic study of the dependency of the ion kinetics on a set of input parameters with respect to expanding structures and their propagation to disentangle individual influences. The considered set of parameters are the main and background plasma density, the electron temperature, the ion mass, and neutral gas properties. The results are qualitatively compared with independent predictions by expansion theories and models.

II. SIMULATION

The PIC code and the used simulation setup is equal to the second setup described in Ref. [2]. In summary, the simulation domain is divided into two regions, the source region and the expansion region resembling the expansion chamber in the plasma expansion experiment[1]. The initial plasma is homogeneous with an electron temperature of $T_\mathrm{e} = 0.5\,\mathrm{eV}$ and an ion temperature at approximately room temperature $T_\mathrm{i} = 0.026\,\mathrm{eV}$ ($T_\mathrm{n} = 300\,\mathrm{K}$ neutral gas temperature). In the source region a high neutral gas pressure at $p_\mathrm{s} = 1\,\mathrm{Pa}$ and an inductive rf-field leads to significant electron impact ionisation collisions. Although the collisionality in the source region is significant, the neutral gas pressure in the expansion region can have much smaller values p_c allowing for a collisionless expansion of the plasma.

III. SYSTEMATIC PARAMETER SCAN

An important issue is the sensitivity of the expansion results with regard to the operation parameters. The total set of configuration parameters of the PIC simulation has been reduced to a limited set of seven parameters. The parameters are the input rf-power P, the background plasma density n_b, and neutral gas parameters. The neutral gas properties are the atom mass m_i, the collision cross sections (adjusted by a scaling factor s_c), the gas pressure in the expansion region p_c, the gradient of pressure profile defined by the width w_n, and the expansion velocity v_n. They are compiled in table I for their default values and parameter range. The parameters are generally chosen in order to analyse their impact on the expansion process. The power and the collisional scaling factor, however, are varied in order to analyse the effect of

parameter	symbol/unit	default	value range
rf-power (n_m)	P/P_0	1	1, 2, 4, (3, 10)
ion mass	m_i/u	40	10, 40, 160
scaling-factor	s_c	1	0.5, 1, 2
backgr. density	$n_\mathrm{b}/10^{13}\,\mathrm{m}^{-3}$	2	0, 1, 2, ..., 19
gas pressure	$p_\mathrm{c}/\,\mathrm{Pa}$	10^{-3}	10^{-3}, 10^{-2}, 10^{-1}, ...
gas front width	$w_\mathrm{n}/\,\mathrm{mm}$	0	0, 10, 20, 30, 40, 50
gas velocity	$v_\mathrm{n}/c_\mathrm{n}$	0	0, 1, 2, ...

TABLE I. List of parameters that are analysed.

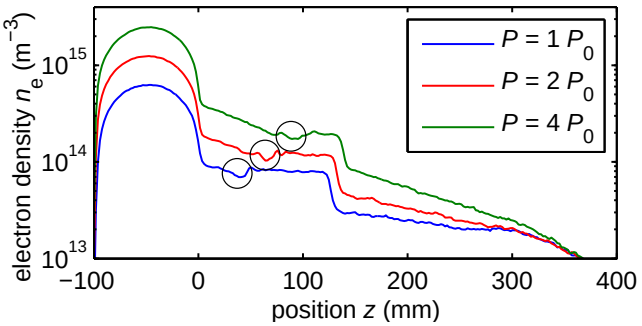

FIG. 1. The electron density profiles for different power values P at $t = 30\,\mu$s.

secondary parameters: the main plasma density and the electron temperature. The expansion dynamics occur on the scale of the ion sound speed, which mainly depends on the electron temperature and ion mass. By altering the background plasma density and rf-power, different ratios of main and ambient plasma density can be simulated. The neutral gas properties have an influence on the initial ion density gradient. The initial ion density gradient is reported to have an impact on the maximum ion velocities[22]. A general description of the expansion mechanics and the used terminology is provided in part I[2].

A. Main plasma density

The rf-power is varied between three different values. For comparison, the resulting electron density profiles for the simulation time instant $t = 30\,\mu$s are depicted in figure 1. The profiles show that an increase of the power is increasing the main plasma density n_m. The plateau (the region of intermediate density between ion front and main plasma[2]) plasma density n_p scales with the main plasma density, however, less than linear. The expanding plasma is separated by a dip in the plasma density (circles). Upstream of that dip the density profile shows a clear gradient. This gradient vanishes downstream of the dip where a plateau of homogeneous plasma density evolves. The density dip is correlated with a vortex in ion phase space that has formed during a wave-breaking event in the early phase of the expansion[2–4]. The propagation velocity of dip and vortex is higher, the higher

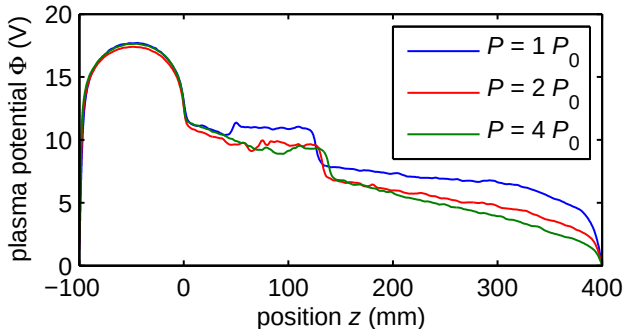

FIG. 2. The plasma potential profiles for different power values P at $t = 30\,\mu$s.

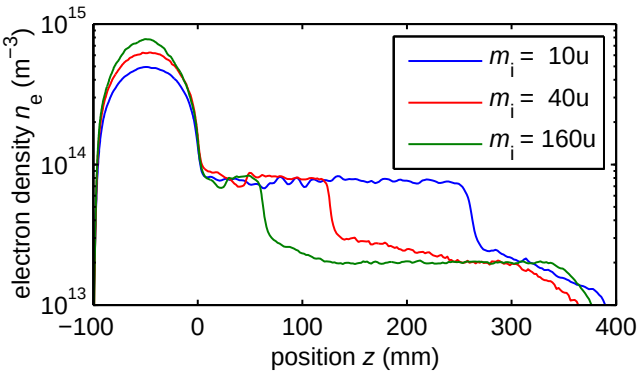

FIG. 3. The electron density profiles for different ion masses m_i at $t = 30\,\mu$s.

the main plasma density. The respective increase of the ion front velocity is much less pronounced. This leads to a broader transition region and a narrower plateau, where the plasma density is roughly constant. The relative density drop at the source edge remains constant. The plasma potential profiles are depicted in figure 2 for comparison. The electron temperature T_e and the plasma potential Φ of the main plasma are unaffected. The discrepancy of the profiles is limited to the regions downstream of the vortex.

B. Ion mass

In figure 3 the electron density profiles for three different values of the ion mass are presented. The profiles show a small discrepancy in the main plasma density and a strong difference in the extension of the plateau region. The plateau front velocity v_f is often observed to scale with the ion mass m_i as $v_\mathrm{f} \propto m_\mathrm{i}^{-1/2}$. For a better comparability, the time vectors can be normalised by the the plasma frequency $\omega_\mathrm{p} \propto m_\mathrm{i}^{-1/2}$. Once normalised the front positions of the three configurations become aligned. The main plasma peak densities have the ratios $1.3 n_{10} \approx n_{40} \approx n_{160}/1.3$. The power can be adjusted accordingly and all three density profiles become identical.

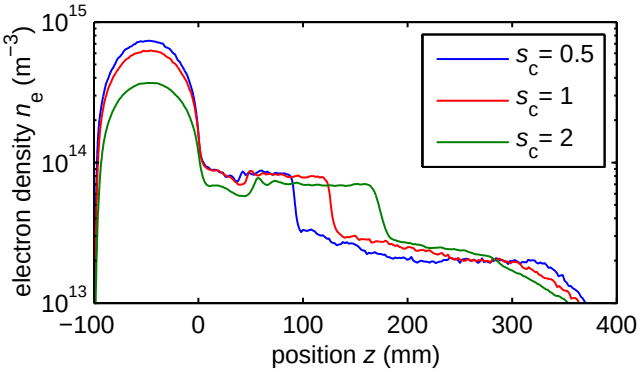

FIG. 4. The electron density profiles for different electron temperatures $T_e(s_c)$ at $t = 30\,\mu$s.

The electron temperature profiles are self-similar with ratios $T_{e10}/3.5 \approx T_{e40}/3.3 \approx T_{e160}/3.1$. This is reflected in the plasma potential profiles, according to BOLTZMANN's relation. However, a significant change of the normalised plateau front velocity is not observed.

C. Electron temperature

The the self-consistently electron temperature can be modified indirectly by altering the energy requirement for electron impact ionisation and excitation collisions via the cross section data s_c as illustrated in Fig. 4. The parameter s_c linearly scales the energy axis of the collision-cross section data that is used in the collision model of the code. The at higher value for s_c, the more kinetic energy of the particles is required for the same collision probability. Due to the neutral gas density profile, the scaling factor mainly influences the source region. The scaling of the electron temperature is more than proportional to s_c. The main plasma electron temperature T_e/s_c obtained by the variation of the electron velocity in the source region is approximately 1.5/0.5, 3.3/1, and 7.5/2, respectively. Figure 4 shows the electron density profiles for three different values of the scaling factor s_c. If the influence on the main plasma density is compensated by altering the input power value, the plateau front velocity scales proportional with $\sqrt{T_e}$. However, this does not hold for the ion stream velocity as one can observe in the ion velocity distribution functions[2]. The ion velocity of the ambient plasma increases towards the front resulting in a decreased relative velocity. The superposition of repelled ions and background ions allows for a local increase of the plasma density with a negative gradient. This gradient gives rise to an electric field proportional to the electron temperature that is accelerating the ambient ions. The velocity of the ambient ions is gradually increasing towards the front. Their velocity just before reflection v_0 depends on the delay between plateau front and ion burst. Since the ion burst is faster, this delay is increasing over time and leads to an increase of v_0. The

s_c	T_e	c_s	v_0	v_f	$2\,v_f - v_0$	v_s	v_f/c_s
0.5	1.5	1.9	0.5	3.0	5.5	5.5	1.58
1	3.3	2.9	0.7	4.4	8.1	8.0	1.54
2	7.5	4.3	0.9	6.3	11.7	11.8	1.47

TABLE II. Relation of the reflection velocities (T_e in eV, velocities in km/s).

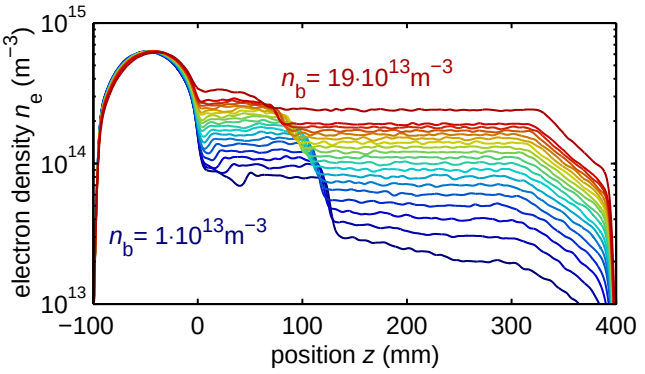

FIG. 5. The electron density profiles for different background densities n_b at $t = 30\,\mu$s.

stream velocity just after reflection is determined by

$$v_s = v_0 + 2\,(v_f - v_0) = 2\,v_f - v_0\,. \qquad (1)$$

Therefore, the velocity of the repelled ions is lower than twice the front velocity and temporally decreasing. The different velocities are compiled in table II and show a good agreement with Eqn. (1) for the three cases. Apart from a broadening of the velocity distribution relative to the ion drift velocity, the ion velocity distribution functions show only minor differences form the default setup[2]. This is because the vortex velocity scales with the electron temperature as well as indicated by the relative position of the density dip in the plateau. The MACH-number of the front, the front velocity v_f normalised to the ion sound velocity c_s, is around 1.5. The accumulation of the ambient plasma leads to a reduction of the potential drop $\Delta\Phi$ at the front, which is approximately given by $e\Delta\Phi \approx k_B T_e$.

D. Background plasma density

The background plasma density n_b set up in the simulation corresponds to the electron density of the ambient plasma n_a. The electron density profiles for different background plasma densities are shown in figure 5. The background density ranges from $1{\cdot}10^{13}\,\mathrm{m}^{-3}$ to $19{\cdot}10^{13}\,\mathrm{m}^{-3}$. The main plasma density profile is unaffected. A higher background plasma density increases the plateau plasma density. This results in a reduced potential drop between main and plateau plasma. The ions acceleration is reduced resulting in a lower plateau front velocity.

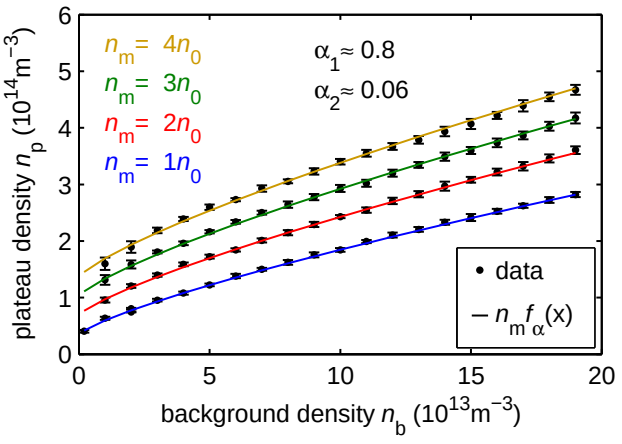

FIG. 6. Fit of Eqn. (2) to the simulation data for four different main plasma densities n_m.

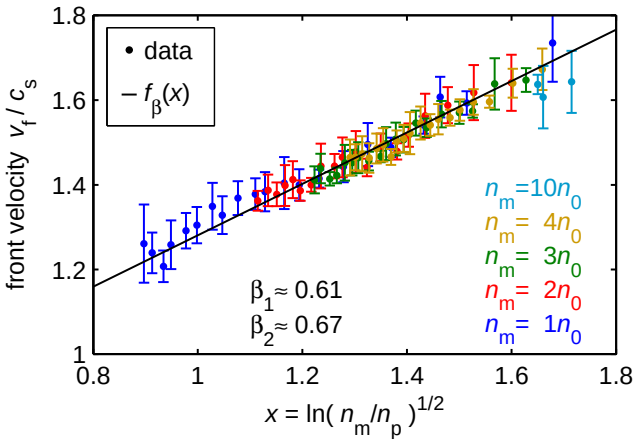

FIG. 7. (a) The plateau front velocity versus the scaling of Eqn. (3). The different ratios $n_\mathrm{m}/n_\mathrm{p}$ arise from the use of different powers and background plasma densities.

Unlike in the cold-ion model[10], not all ambient ions are reflected by the plateau front. At $n_\mathrm{b} = 1{\cdot}10^{13}\,\mathrm{m}^{-3}$ approximately one third of the ambient ions are reflected. The ratio drops almost exponentially with the background plasma density to only 5% at $n_\mathrm{b} = 8{\cdot}10^{13}\,\mathrm{m}^{-3}$. The unreflected ions contribute to the plateau plasma density n_p which can be described by an empirical function

$$n_\mathrm{p}(n_\mathrm{m}, n_\mathrm{b}) = n_\mathrm{m}\, f_\alpha\left(\frac{n_\mathrm{b}}{n_\mathrm{m}}\right), \qquad (2)$$

with $f_\alpha(x) = x^{\alpha_1} + \alpha_2$, where α_1 and α_2 are fit parameters. Figure 6 shows the fit to a set of simulation results with different background and main plasma densities. The four curves correspond to four values for the main plasma density. The obtained fitting parameters are universal for all values for n_m with $\alpha_1 \approx 0.8$ and $\alpha_2 \approx 0.06$. In the vacuum limit ($n_\mathrm{b} \to 0$), Eqn. (2) reduces to $n_\mathrm{p} = n_\mathrm{m}\alpha_2$ and α_2 relates to the source edge plasma density. The value for α_2 is approximately one third of the source edge plasma density.

The maximum plasma potential in the main plasma remains constant at $\Phi_\mathrm{m} = 15\,\mathrm{V}$ throughout the setups. The difference in the plateau plasma density influences the plateau potential following Boltzmann's relation. In result, the electric field in the transition region between main and plateau plasma varies, leading to different velocities of the plateau front. The kinetic energy of the plateau ions increases roughly proportional with the potential drop in the transition. Thus, the front velocity v_f is expected to scale as

$$\frac{v_\mathrm{f}}{c_\mathrm{s}} = f_\beta\left(\sqrt{\ln\left(\frac{n_\mathrm{m}}{n_\mathrm{p}}\right)}\right), \qquad (3)$$

with $f_\beta(x) = \beta_1 x + \beta_2$, where β_1 and β_2 are fit parameters. The relation can be fitted to the simulation data and is depicted in figure 7. Each setup given in figure 6 is represented by a data point and the respective error bar.

curve	$f(x)$	$f(0)$	$f(1)$	δ_1	δ_2	α_1	α_2
–	$f_\delta(x)$	1.71	1.07	−0.64	1.71	-	-
..	$f_{\delta\alpha}(x)$	1.71	1.10	**−0.64**	**1.71**	**0.78**	**0.06**
–	$f^*_{\delta\alpha}(x)$	1.69	0.99	−0.74	1.69	0.37	0.06
..	$f^*_\delta(x)$	1.69	0.95	**−0.74**	**1.69**	-	-

TABLE III. Coefficients and extrapolation for the fit of Eqn. (4) and (5) depicted in figure 8 and 8b, respectively. The bold coefficients are set as constant parameters. δ_1 and δ_2 are taken from the respective previous fit. α_1 and α_2 are taken from the fit of Eqn. (2).

The saturation plateau plasma density n_p and the front velocity v_f are linked by the ion flux. Thus, if the plateau plasma density decreases at lower background plasma densities, a higher front velocity is expected. The ratio between background n_b and plateau plasma density n_p has a significant influence on the front. A higher background plasma influences the initial plasma potential drop noticeably and thereby reduces the ion acceleration. The kinetic energy remains in the electrons that can overcome the plateau front potential drop more and more easily. The change of the ion front velocity with changing background plasma density is depicted in figure 8a and 8b. Each graph shows different setups covering different power and background plasma density parameters. The ion front velocity v_f is normalised to the respective ion sound speed. In figure 8a, it is plotted against the plasma density ratio $x = n_\mathrm{b}/n_\mathrm{p}$. The empirical fit (solid line) is given by the linear function:

$$f_\delta(x) = \delta_1\, x + \delta_2\,, \qquad (4)$$

where δ_1 and δ_2 are fit parameters. The respective function in $x = n_\mathrm{b}/n_\mathrm{m}$ used in figure 8b can be obtained with the use of Eqn. (2):

$$f_{\delta\alpha}(x) = \delta_1\, x\,(x^{\alpha_1} + \alpha_2)^{-1} + \delta_2\,. \qquad (5)$$

The solid lines represent the direct fits of Eqn. (5) and (4) to the data. The dotted lines are for comparison and

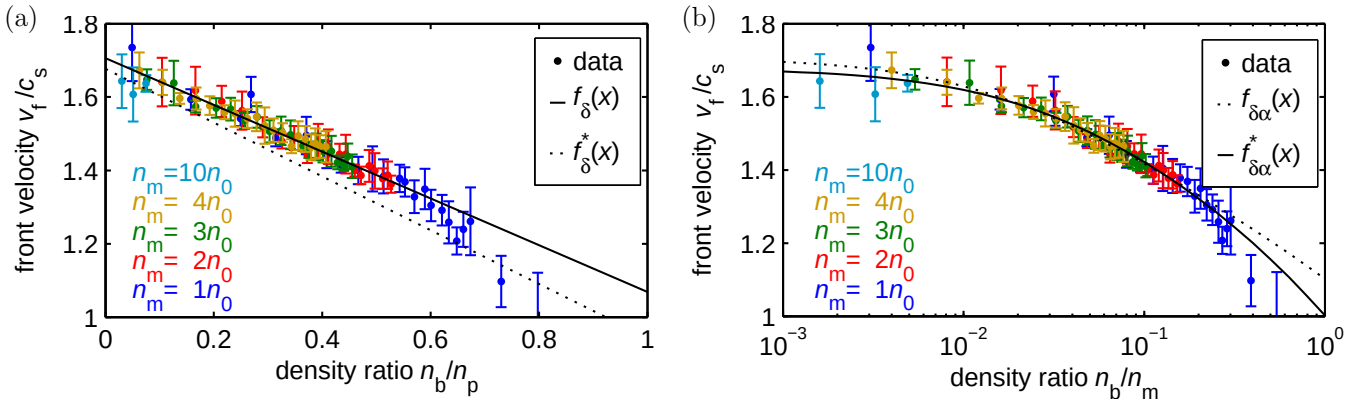

FIG. 8. Front velocity v_f normalised to the ion sound velocity as function of the background plasma density normalised to (a) the plateau and (b) the main plasma density. The fits are given by Eqn. (4) and (5), respectively. The resulting coefficients are compiled in table III

represent respective curves using the parameters compiled in table III. Both fits extrapolate to $v_f \approx 1.7\,c_s$ for $n_b = 0$ and to $v_f \approx 1\,c_s$ for $n_b = n_m$. The unity limit $v_f = c_s$ resembles the propagation velocity of small density perturbations in an isothermal plasma, which is well understood[23]. The value for $\delta_2 \approx 1.7$ is in good agreement with the adiabatic expansion of arc discharges[14,24]. The expansion of plasma into a low density background plasmas yields in a plateau front velocity of $v_f \approx 1.45\,c_s$ if the velocity space is restricted to two dimensions. This value fits well with the adiabatic model[14] ($v_f \approx \sqrt{2}\,c_s$). However, since the electron temperature is maintained by the source, the expansion can be considered as isothermal. This indicates an only coincidental agreement with the adiabatic expansion model.

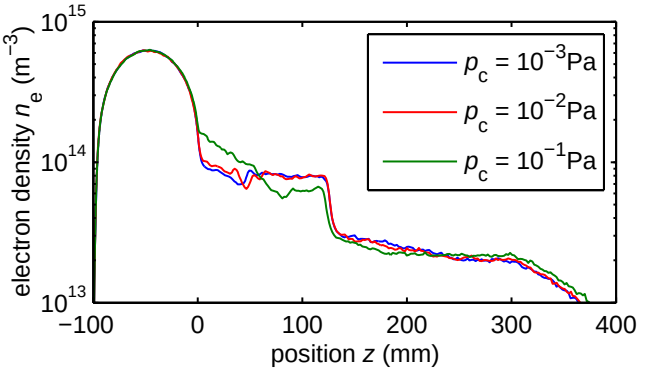

FIG. 9. The electron density profiles for different neutral gas pressures in the expansion region p_c at $t = 30\,\mu$s.

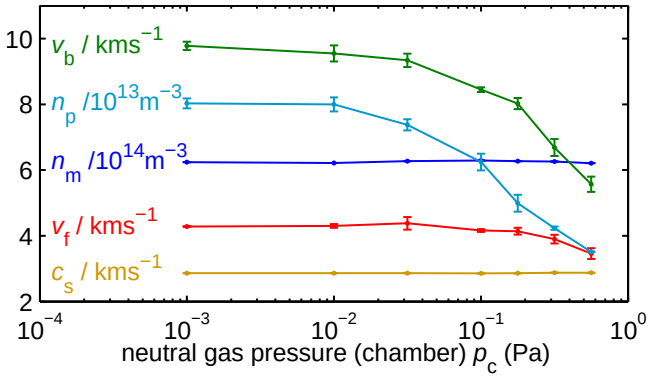

FIG. 10. Different parameters against the pressure of the neutral gas in the expansion region p_c at $t = 30\,\mu$s.

E. Background neutral gas pressure

The neutral gas pressure in the expansion region p_c resembles the background gas pressure in the expansion experiment prior to the gas injection[1]. At low plasma density, it predominantly influences the collisionality during the expansion. Figure 9 shows the plasma density profiles for three different values of p_c. The influence of collisions on the expansion is rather complex. The collisionality does not directly influence the expansion, but it influences the plasma density profile. A high collisionality in the chamber decreases the plasma density gradient due to local electron impact ionisation. Without a sharp plasma density gradient the formation of the vortex gets distorted and it smears out into the plateau. At $p_c = 10^{-1}$ Pa the plasma density profile shows a much more pronounced exponential transition region between source and the shortened plateau region. The drifting ions in the plateau constantly lose density due to collisions. The loss is eventually balanced by absorbed ambient ions and local electron impact ionisation and the plateau plasma density n_p remains constant over time.

The relation between n_p and the chamber gas pressure p_c can be described by:

$$n_p(p_c) = \sqrt{n_b^2 + n_{p0}^2 f_\eta\left(\frac{p_c}{p_s}\right)}, \qquad (6)$$

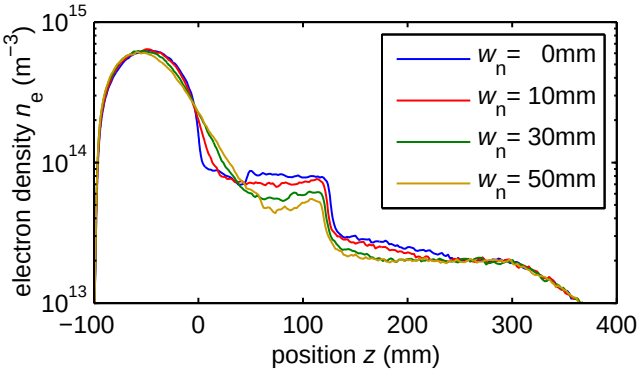

FIG. 11. The electron density profiles for different neutral gas front widths w_n at $t = 30\,\mu$s.

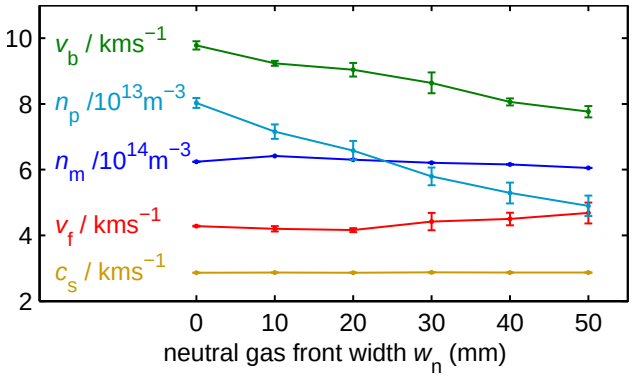

FIG. 12. Different parameters against the width of neutral gas front w_n at $t = 30\,\mu$s.

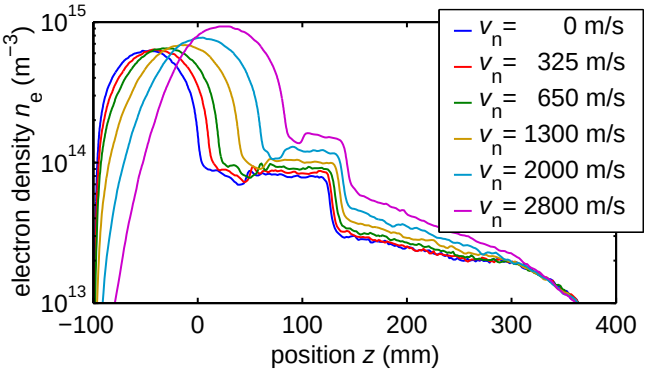

FIG. 13. The electron density profiles for different neutral gas expansion velocities v_n at $t = 30\,\mu$s.

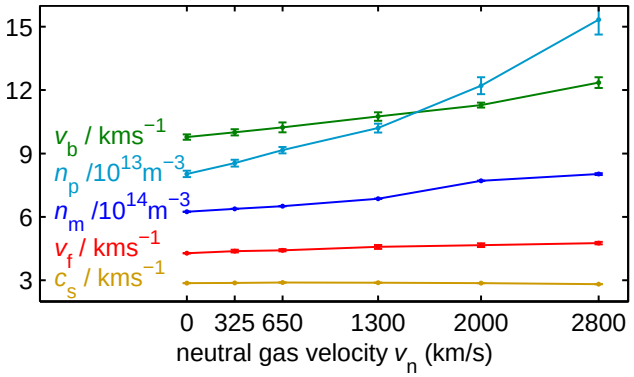

FIG. 14. Different parameters against the neutral gas expansion velocity v_n at $t = 30\,\mu$s.

with $f_\eta(x) = \left(\eta_1 + \eta_2\, x + \eta_3\, x^2\right)^{-1}$ [25] and $n_{p_0} = n_p(0)$. It drops down to the background plasma density n_b when the chamber gas pressure approaches the source gas pressure p_s. The background plasma is a required initial condition in the simulation, and one can assume that, even for the collisionless experiment, the plasma density in the expansion chamber is non-zero. This is due to the non-zero electron impact ionisation frequency in the low pressure region, which scales with the neutral gas density. The dependency of the different density levels and velocities are compiled in figure 10. The peak plasma density n_m and the electron temperature T_e represented by the ion sound velocity c_s remain constant. However, the plateau density n_p and the ion burst velocity v_b are strongly reduced at higher background gas pressures p_c due to ion-neutral collisions.

F. Neutral gas front width

The gas front width w_n influences the initial plasma density gradient in the transition from the source to the expansion region by determining the ionisation probability. A sharper neutral gas front results in a steeper plasma density gradient as depicted in figure 11. A smooth neutral gas front allows for more ionisation events in the expansion region to the expense of ionisation events in the source region around the transition. It further results in a smooth transition to a less pronounced plateau plasma. The decrease of the plateau plasma density directly correlates with a decrease of the plasma density drop at the plateau front. The related reduction of the initial plasma potential gradient leads to a decrease of the ion burst velocity. The neutral gas front width has a strong impact on the vortex formation and the collisionality in the plateau but has no influence on the plateau front velocity. In figure 12 the critical parameters are plotted against the neutral gas front width w_n. The plasma peak density, the electron temperature, and the ion front velocity are independent of the front width. The pedestal density and the ion burst velocity, however, reach higher values the sharper the neutral gas front.

G. Neutral gas expansion velocity

The neutral gas expansion velocity v_n can have a huge impact on the plasma parameters since it technically increases the ionisation region over time. This influence can clearly be seen in the plasma density profiles de-

picted in figure 13. It results in a higher peak plasma density over time. During the ignition phase, the propagation of the neutral gas front leads to a decrease of the plasma density gradient. This reduces the acceleration of the burst ions. However, since the burst ions mainly origin from ionisation events, their initial drift velocity is given by the velocity of the neutrals. The decrease of the initial plasma gradient is practically negligible. The development of the key parameters when going to higher neutral gas velocities v_n is depicted in figure 14. The pedestal density increase is significant at higher values of neutral drift velocity. The higher plateau density results in a more pronounced ion front, a higher reflection ratio of the front, and a higher ion stream density, which adds up with the accumulated ambient plasma density. The increase of the ion front velocity is insignificant with less than 10%. In the related expansion experiment[1] the neutral drift is on the order of the neutral sound velocity and its effects are negligible on the time scale of the plasma expansion.

IV. DISCUSSION

From the parameter scan, one can deduce a hierarchy of parameters that influence the expansion behaviour, especially in terms of the expansion velocity. For the plateau front velocity v_f, the proportionality can be verified to be $v_\mathrm{f} \propto \sqrt{T_\mathrm{e}/m_\mathrm{i}}$, which is just proportional to the ion sound velocity $c_\mathrm{s} = \sqrt{k_\mathrm{B} T_\mathrm{e}/m_\mathrm{i}}$. The front velocity is super sonic and can become as high as $v_\mathrm{f} \approx 1.7\, c_\mathrm{s}$. The ion stream, which consists of ions reflected by the plateau front, is up to twice as fast. The initial velocity after reflection is reduced over time due to the acceleration of the ambient ions prior to the front arrival. The acceleration is due to the additional ions of the ion stream, which result in the generation of an electric field. The maximum ambient ion velocity is the front velocity itself. However, the generated ion stream experiences an accelerating electric field again and approaches the original stream velocity of $2\, v_\mathrm{f}$. The fastest ions form the ion burst that is generated in the very early phase of the rf power pulse. For a potential drop on the order of the electron temperature, the burst velocity is on the order of $v_\mathrm{b} \approx 3\, c_\mathrm{s}$, but due to the increased potential drop in the initial phase, the burst velocity is usually much higher[22].

The maximum potential drop can be influenced by changing the main plasma density, the background plasma density, or the gradient of the neutral gas density given by w_n. The highest burst velocities are observed in the absence of a background plasma. In the initial phase of the pulse, while the plasma density in the source is still very low, the energy input per electron scales with the rf-power and increases the electron temperature. As a result, the plasma potential and the initial potential drop is increased. The initial potential drop is significantly affecting the ion burst velocity. The trend is clearly visible

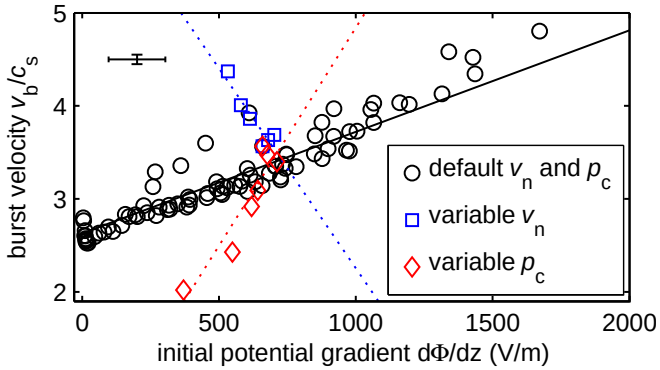

FIG. 15. The ion burst velocities v_b at $t = 30\,\mu$s against the initial plasma potential gradient $\mathrm{d}\Phi/\mathrm{d}z$ during the first $1\,\mu$s. The error bars in the top left corner resemble the mean values of the respective standard deviations.

in figure 15 showing a collection of setups of the parameter scan (circles) except for ones with a non-zero neutral gas velocity (squares) and the higher chamber pressure (diamonds) as these parameters have a direct influence on the ion burst velocity. The neutral gas drift velocity adds to the ion burst velocity, whereas a high neutral gas pressure in the chamber additionally reduces the maximum ion velocity due to ion-neutral collisions.

The plateau front velocity has a strong correlation with the ion flux that is ejected from the main plasma. As a consequence the plateau plasma density is determined by the main plasma density as well as by the ambient plasma density. The main plasma behaves as if the plateau would be a boundary with absorbing capabilities determined by the ambient plasma density. A robust prediction of the expected plateau plasma density is given by Eqn. (2). The plateau front velocity strongly depends on the ion mass and the main plasma electron temperature $v_\mathrm{f} \propto \sqrt{T_\mathrm{e}/m_\mathrm{i}}$ indicating its relation to the ion sound velocity. This in agreement with observations that have been made e.g. during arc discharges[14]. However, the ratio of the ion front velocity to the ion sound speed drops with the ratio of ambient to main plasma density.

In summary, this paper has presented a parameter study on expanding plasma. The expansion of plasma is characterised by a sharp density gradient associated with strong electric fields as given by the Boltzmann relation. The electric field accelerates the ions in direction of the expansion (downstream) and a propagating ion front is formed.

The existence of such ion fronts has previously been confirmed for rf-discharges[1]. The presented parameter study has been carried out with the use of a particle in cell simulation that has been tailored to the corresponding experimental setup[2]. It has been used to analyse the influence of the main and ambient plasma density, the electron temperature, the ion mass, and different neutral gas properties on the expansion dynamics, in particular on the ion ejection velocities. The expansion of plasma

into an ambient plasma of lower density features the formation of a plasma density plateau[2]. The plateau is a region of approximately constant density. The analysis has shown, that its density is determined by the ratio between main and ambient plasma density. Upstream, the plateau is terminated by a vortex in ion phase space that forms at the intersection with the main plasma. Within the vortex, the propagation velocity of the expanding ions coming from the source is limited. This results in a constant ion drift velocity throughout the plateau. For larger ratios between the main and the ambient plasma density, the vortex is propagating downstream, and the plateau becomes less pronounced. The expansion of a semi-infinite plasma into an ambient plasma with high density ratios ($n_\mathrm{m}/n_\mathrm{a} = 100$) has been investigated independently using a different PIC simulation with periodical boundary conditions[24]. The shortening of the plateau and the transition to the vacuum case is found in both PIC simulations. A rarefaction-wave into the high density region is not observed since the simulated source prevents its formation. The agreement of the relative front velocities in both simulation approaches indicates that the rarefaction-wave is a truly independent phenomenon. In analytical models this is reflected in the constant electron density and ion drift velocity at the origin[6].

The intersection between the plateau and the ambient plasma is given by a sharp density drop, the plateau front. The plateau front propagates with a velocity approximately equal to the plateau drift velocity. In addition to the well known dependencies, i.e. the electron temperature T_e and the ion mass m_i related by the ion sound velocity $c_\mathrm{s} = \sqrt{k_\mathrm{B} T_\mathrm{e}/m_\mathrm{i}}$, the propagation velocity is strongly influenced by the density of the ambient plasma. It is shown that this relation can be described by a non-linear function. The plateau front velocity ranges from the ion sound speed for a density ratio close to unity and up to $1.7\,c_\mathrm{s}$ in the vacuum limit. For density ratios close to unity, the physical problem reduces to the well understood propagation of ion acoustic waves[26]. Under the isothermal conditions given in the PIC simulation, the ion front velocity approaches the ion sound velocity as expected. The value for the vacuum limit agrees well with the experimentally observed value for the adiabatic expansion of arc discharges[14].

The propagating electric field structure that is associated with the plateau front is accelerating the ambient ions while it is passing by. The reflected ions form a narrow ion stream with stream velocities up to twice as high as the propagation velocity of the front, similar to the Fermi acceleration mechanism[27]. The ion stream is tipped by the ion burst resembling the fast ion peak, i.e. the ion front in the vacuum expansion[6]. The ion burst density is gradually decreasing due to its velocity spread and eventually becomes negligible compared to the ambient plasma density. The electric field at the ion burst vanishes resulting in a saturation of the ion burst velocity. The maximum velocity of the ion burst can be much higher than the ion stream velocity as it is determined by the maximum potential gradient. Thus it depends mainly on parameters that affect the initial density gradient at the source chamber intersection, i.e. the rf-power, the neutral gas front width and chamber pressure. The ion burst velocity is further increased by the drift velocity of the neutrals upon their ionisation. This qualitatively confirms observations that have been made with an independent PIC simulation[24], however with different saturation values for the burst velocity. The much sharper potential gradient in that semi-infinite PIC simulation is presumably the reason for the 60% velocity increase compared to our results. The associated plasma expansion experiment has provided evidence for the existence of the ion stream in form of a propagating front. The energy analyser has clearly shown two different drift velocities downstream and upstream of the plateau front[1]. The respective drift velocities match with the expected values for the ion front and ion stream velocity within a relative error of only 10%. The comparison of the front and stream velocities with the results from a Vlasov-Poisson model[10] shows that both approaches agree quantitatively within a deviation of much less than 10%.

ACKNOWLEDGMENTS

The author would like to thank the DAAD (German Students Exchange Service) for funding and the colleagues of the RSPE, ANU, Canberra for their support and hospitality. This work has been carried out within the framework of the EUROfusion Consortium and has received funding from the European Unions Horizon 2020 research and innovation programme under grant agreement number 633053. The views and opinions expressed herein do not necessarily reflect those of the European Commission.

[1] T. Schröder, O. Grulke, T. Klinger, R. W. Boswell, and C. Charles, J. Phys. D: Appl. Phys. **47**, 055207 (2014).
[2] Submitted as Part I: MS# POP46666 Collisionless expansion of pulsed rf plasmas I: Front formation
[3] C. Sack and H. Schamel, Plasma Phys. Control. Fusion **27**, 717 (1985).
[4] C. Sack and H. Schamel, Phys. Lett. A **110**, 206 (1985).
[5] J. E. Allen and J. G. Andrews, J. Plasma Phys. **4**, 187 (1970).
[6] J. E. Crow, P. L. Auer, and J. E. Allen, J. Plasma Phys. **14**, 65 (1975).
[7] A. V. Gurevich, I. V. Pariiska, and L. P. Pitaevskii, Sov. Phys. JETP **22**, 449 (1966).
[8] M. Widner, I. Alexeff, and W. D. Jones, Phys. Fluids **14**, 795 (1971).
[9] P. Mora and R. Pellat, Phys. Fluids **22**, 2300 (1979).
[10] M. Perego, P. D. Howell, M. D. Gunzburger, J. R. Ockendon, and J. E. Allen, Phys. Plasmas **20**, 052101 (2013).
[11] G. Hairapetian and R. L. Stenzel, Phys. Rev. Lett. **61**, 1607 (1988), phD.
[12] G. Hairapetian and R. L. Stenzel, Phys. Fluids B **3**, 899 (1991).
[13] R. L. Stenzel, C. Ionita, and R. Schrittwieser, Plasma Sources Sci. Technol. **17**, 035006 (2008).
[14] H. W. Hendel and T. T. Reboul, Phys. Fluids **5**, 360 (1962).

[15]G. M. W. Kroesen, D. C. Schram, A. T. M. Wilbers, and G. J. Meeusen, Contrib. Plasma Phys. **31**, 27 (1991).
[16]A. V. Gurevich and A. P. Meshcherkin, Sov. Phys. JETP **53**, 1810 (1981).
[17]B. Bezzerides, D. W. Forslund, and E. L. Lindman, Phys. Fluids **21**, 2179 (1978).
[18]J. S. Pearlman and R. L. Morse, Phys. Rev. Lett. **40**, 1652 (1978).
[19]J. Denavit, Phys. Fluids **22**, 1384 (1979).
[20]A. V. Mordvinov, V. M. Tomozov, and V. G. Fainshtein, J. Appl. Mech. Tech. Phys. **26**, 764 (1985).
[21]M. A. True, J. R. Albritton, and E. A. Williams, Phys. Fluids **24**, 1885 (1981).
[22]T. Grismayer and P. Moras, Phys. Plasmas **13**, 032103 (2006).
[23]T. H. Stix, *Waves in plasmas* (American Inst. of Physics, 1992) iSBN: 978-0883188590.
[24]G. Sarri, M. E. Dieckmann, I. Kourakis, and M. Borghesi, Phys. Plasmas **17**, 082305 (2010).
[25]C. Lee and M. A. Lieberman, J. Vac. Sci. Technol. and A **13**, 368 (1995).
[26]J. E. Allen and A. D. R. Phelps, Rep. Prog. Phys. **40**, 1305 (1977).
[27]E. Fermi, Phys. Rev. **75**, 1169 (1949).